RSC Advances

ROYAL SOCIETY OF CHEMISTRY

www.rsc.org/advances

Graphical Abstract

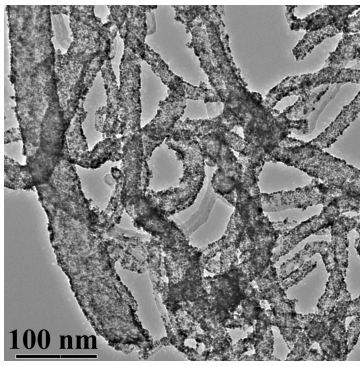

Based on carboxylated-carbon nanotubes (CNT-C) prepared by direct Friedel-Crafts reaction between pristine CNTs and maleic anhydride, PtRu nanoparticles highly dispersed on CNT-C surface and showed superb performance toward methanol electrooxidation.

Journal Name

RSCPublishing

ARTICLE

Tailoring Carbon Nanotubes Surface with Maleic Anhydride for Highly Dispersed PtRu Nanoparticles and Their Electrocatalytic Oxidation of Methanol

Bohua Wu,[a,b*] Chao Wang,[a**] Ying Cui,[c] Liqiu Mao,[c] and Shanxin Xiong,[b]

Cite this: DOI: 10.1039/xoxxoooooox

Received ooth January 2012,
Accepted ooth January 2012

DOI: 10.1039/xoxxoooooox

www.rsc.org/

Taking the direct Friedel-Crafts reaction between pristine carbon nanotubes (CNT) and maleic anhydride, we have developed a facile strategy for synthesis of carboxylated-carbon nanotubes (CNT-C). The covalently grafted enough carboxyl groups on CNT-C not only obviously improve its hydrophilicity, but also effectively anchor and stabilize PtRu nanoparticles. Transmission electron microscope images reveal that PtRu nanoparticles with an average size of 3.3 nm uniformly dispersed on CNT-C surface. Electrochemical results demonstrate the obtained PtRu/CNT-C nanohybrids have higher electrochemical surface area, electrocatalytic activity and better stability towards methanol oxidation compared to PtRu nanoparticles supported on acid oxidized-CNT. This provides a facile approach to synthesize noble metal nanoparticles/CNT electrocatalysts for high performance energy conversion devices in the future.

1. Introduction

Since carbon nanotubes (CNT) were discovered by Iijima in 1991[1], they have been extensively studied and suggested great potential applications in a wide variety of areas, such as fuel cells[2-9], heterogeneous catalysis[10], and chemo/biosensors[11]. Especially, the large specific surface areas, high electric conductivity, outstanding chemical and electrochemical stability make CNT as ideal supporting materials for noble metal nanoparticles, which have shown great promises in advanced sensors and fuel cells[12-23], including direct methanol fuel cells (DMFCs). It is well known Pt is the most popular anode catalyst towards oxidation of methanol; however, it is often easily poisoned by CO intermediate products to gradually decrease their catalytic activity[3, 5, 8]. To improve the electrocatalytic activity and stability, various Pt-based multicomponent catalysts such as PtCo[24], PtSn[25], PtRu[3, 5, 15], PtCu[26], Pt-MnO_2[27], etc. have been investigated. Extensive efforts are still paid to further improvement of electrocatalytic activity of Pt catalysts for their practical applications in DMFCs. Since the properties of electrocatalyst are highly depended on their dispersity and particle size[28-31]. The highly dispersed metal nanoparticles with small particle size on CNT are desired to enhance the performance of fuel cells with low noble metal loadings in engineering applications. Unfortunately, pristine CNT have insufficient accessible specific surface areas and binding sites for anchoring noble metal nanoparticles owing to their poor dispersibility in solvents and insert graphitic surface[3, 14, 32-34]. On the other hand, noble metal nanoparticles are kinetically unstable for agglomeration to the bulk metal and thus further aggravates the difficulty to uniformly deposit noble metal nanoparticles on pristine CNT[28, 30, 35, 36].

To overcome the above problems, great research efforts have been devoted to attach uniform noble metal nanoparticles onto CNT. One of widely used strategies is acid oxidation treatment of CNT to graft carboxyl groups as binding sites for anchoring noble metal nanoparticles[28, 30]. However, because of its limited and uneven distribution of functional groups, noble metal nanoparticles on the acid oxidized-CNT (AO-CNT) generally have large particle size, poor dispersion and agglomeration, which is inferior for gaining high catalytic performance. Meanwhile, noncovalent functionalization methods including wrapping polymers such as poly(vinylpyrrolidone) [32], poly(allylamine hydrochloride) [17], poly(ethyleneimine) [37] onto CNT or modifying CNT with 1-aminopyrene by π-π stacking [38], have attracted particular attention because it can facilely decorate uniform noble metal nanoparticles on CNT surface without structural damage of CNT. However, in most cases, these template agents such as polymer, surfactant and macromolecule can strongly bind to the surface of resulting noble metal nanoparticles and lead to surface poisons in electrocatalytic reaction, which is disadvantageous for enhancing electrocatalytic performance of the nanohybrids. The elimination of template agents from nanohybrids is difficult to perform while still keeping the noble metal nanoparticles' size and dispersion. Thus, it is necessary to develop an effective functionalization method that can attach high dispersion of noble metal nanoparticles with clean surface onto CNT for high electrocatalytic activity.

Recently, Wei *et al.* [39] covalently functionalized CNT with thiol groups (SH-CNT) and highly dispersed Pt nanoparticles on SH-CNT, which displayed good durability and excellent activity for oxygen reduction reaction. Niu and co-workers [40] grafted ionic liquid onto CNT (CNT/IL) and uniformly deposited Au nanoparticles with average diameter of 3.3 nm on CNT/IL, showing significantly strengthened activity for oxygen reduction. These valuable tries inspired us to employ a

controllable reaction under mild conditions which would covalently graft massive and uniform distribution functional groups on CNT surface for dispersing noble metal nanoparticles with clean surface for electrocatalytic reaction. Herein, by selecting PtRu nanoparticles as the model because of wide interest in their use in direct methanol fuel cells, we report a facile pathway for high-efficiency dispersion of noble metal nanoparticles on CNT. Our approach is based on the direct Friedel-Crafts reaction between pristine CNT and maleic anhydride by using aluminium chloride as catalyst to graft carboxyl-terminated groups onto pristine CNT (Scheme 1). The PtRu nanoparticles electrocatalysts with average size 3.3 nm and narrow size distribution were uniformly deposited on the resulting carboxylated-carbon nanotubes (CNT-C) in the following microwave-assisted polyol process. The grafted high-density and uniform distribution carboxyl-terminated groups not only improve the hydrophilicity of CNT to offer enough accessible specific surface areas but also act as binding sites for anchoring metal ions and nanoparticles. More importantly, the short containing-carboxyl chain direct grafted on the carbon atoms of the CNT surface only give rise to a negligible contact resistance between the PtRu nanoparticles and CNT, thus do not affect the electron transport pathway. In addition, our method does not use any template agents, thus the noble metal nanoparticles in the as-prepared nanohybrids have clean surface for electrocatalytic reaction. The resulting PtRu/CNT-C nanohybrids would exhibit superior electrocatalytic activity for methanol oxidation, comparing with PtRu nanoparticles supported on AO-CNT and PtRu/C catalysts reported previously.

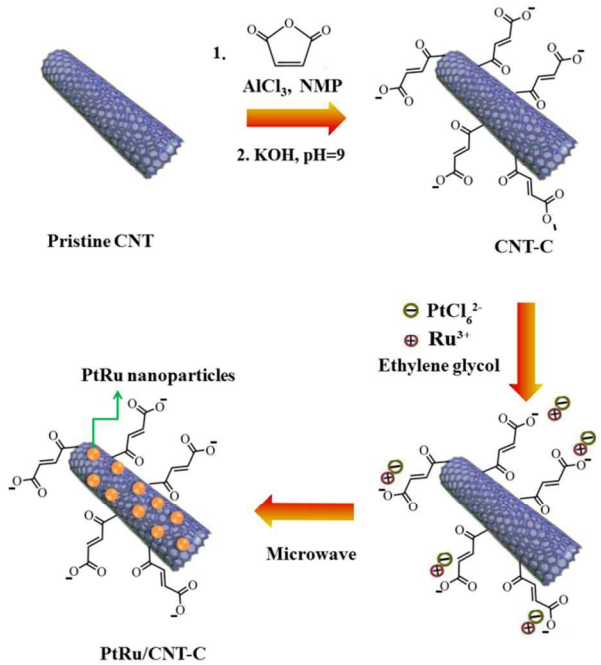

Scheme 1. Schematic diagram of the CNT-C and preparation of PtRu/CNT-C nanohybrids.

2. Experimental

2.1 Materials

Pristine multi-walled carbon nanotubes (CNT) (length 5-15 μm, diameter 20-60 nm) were purchased from Shenzhen Nanotech Port Co. Ltd., China. Maleic anhydride (99%) was purchased from Alfa Aesar. Other chemicals were of analytical grade and used as received.

2.2 Preparation of CNT-C and PtRu/CNT-C catalysts

The preparation procedure for the CNT-C was as follows: Pristine CNT (100 mg), maleic anhydride (1 g) was refluxed with $AlCl_3$ (1.33 g) in dried N-methyl-2-pyrrolidone at approximately 90 ^oC under a dry nitrogen atmosphere for 4 h. Then, the reaction mixture was stirred at 150 ^oC for 48 h. After the reaction, the mixture was decomposed with double-distilled water followed by 0.5 M HCl aqueous solution. The obtained samples were then washed with double-distilled water five times and following adjusted the pH to 9 with 1.0 M KOH aqueous solution. Finally, the filtered solid was dried under vacuum for 12 h at 40 ^oC to obtain CNT-C. The acid-oxidized CNT (AO-CNT) prepared by refluxing pristine CNT in a mixed acid (H_2SO_4:HNO_3 in 1:3 v/v ratio) solution for 5 h, and then washing with double-distilled water until the pH became neutral.

Deposition of PtRu nanoparticles on CNT-C was carried out via microwave-assisted reduction process in ethylene glycol solution. The details were as follows: 20 mg of CNT-C was mixed with 438 μL H_2PtCl_6 (38.6 mM) in ethylene glycol solution. After ultrasonication for 15 min, 350 μL $RuCl_3$ (48.2 mM) was added into above mixture and ultrasonic blended for 30 min. Then, the pH value of the solution was adjusted to 8-9 with 1.0 M KOH aqueous solution. The mixture was placed in a microwave oven and heated by microwave irradiation (800 W) for 30 min at 120 ^oC. The products were centrifuged and washed three times with distilled water. The obtained sample denoted as PtRu/CNT-C, were dried in vacuum oven at 60 ^oC for 12 h. For comparison, PtRu nanoparticles supported on the AO-CNT, labeled as PtRu/AO-CNT, were prepared under the same procedure as described above.

2.3 Physical characterization of the electrocatalysts

The metal Pt and Ru loading mass for the PtRu/CNT-C (or PtRu/AO-CNT) catalyst was determined by Inductively Coupled Plasma-Atom Emission Spectroscopy (ICP-AES, Spectro Ciros) and the corresponding results were shown in Table *S1*. Fourier transform infrared spectrometry (FTIR, Nicolet 6700) and X-ray Photoelectron Spectrometer (XPS) (AXIS ULTRA, Kratos Analytical Ltd., Japan) were employed to analyze the surface chemical compositions of the CNT-C. The present FTIR study uses the traditional KBr pellet and pellets were prepared from a mixture of sample and KBr at a 1:100 (wt.:wt.) ratio. The Raman spectrum (in Via, Renishaw, England) was also used to study the integrity and electronic structure of the samples. The morphology and structure of PtRu/CNT-C and PtRu/AO-CNT catalysts were characterized by transmission electron microscopy (TEM, JEOL 3010, 200kV) and powder X-ray diffraction (XRD, Bruker AXS X-ray diffractometer), respectively.

2.4 Electrochemical measurements of the electrocatalysts

For electrochemical investigation, a glassy carbon (GC, 5 mm diameter) electrode was polished with the slurry of 0.5 and 0.03 μm alumina successively and washed ultrasonically in double-distilled water prior to use. The catalyst ink was prepared by dispersing 5 mg of catalyst in 5 mL of water by sonication. When a dark homogeneous dispersion was formed, 40 μL of the ink was dropped onto the GC electrode using micro-syringe. After dried in air, the electrode was coated with 10 μL of 0.05 wt. % Nafion ethanol solution to fix the catalyst powder. The electrochemical surface area (ESA) and the electrochemical performance of the electrocatalysts were evaluated by cyclic voltammetry. All electrochemical measurements were performed on a CHI660D electrochemical

workstation (Chenhua Instrument Company of Shanghai, China). A conventional three-electrode glass cell was used with a platinum wire as the counter electrode and a saturated calomel electrode (SCE) as the reference electrode. All the potentials reported herein were in respect to SCE. Double-distilled water was used throughout.

3. Results and discussion

Characterization of CNT-C support– Surface-functionalization of CNT was characterized by FTIR spectroscopy. The FTIR spectra of maleic anhydride, pristine CNT and CNT-C are shown in Figure 1. In the FTIR spectrum of maleic anhydride, the characteristic bands at 900 cm^{-1} was assigned to C-O-C of MA group (curve 1 in Figure 1). The characteristic peaks at 1596 cm^{-1} the ν(C-H) stretching vibration and peaks at 1850 and 1784 cm^{-1} was the asymmetric and symmetric vibration of ν(C=O), respectively. The pristine CNT has no obvious characteristic absorption peaks since their very few functional groups (curve 2 in Figure 1). For the FTIR spectra of CNT-C (curve 3 in Figure 1), there is no peak at 900 cm^{-1}, which confirms that the five membered rings are completely opened. The peaks at 1600 and 1417 cm^{-1} are assigned to the asymmetric and symmetric stretching vibration of $\nu(COO^-)$ in carboxylate ion. One broad peak at 3423 cm^{-1} should be ascribed to ν(O-H) stretching vibration of the absorption of water in CNT-C. This result revealed the presence of carboxylate ion on CNT-C and the successful functionalization of CNT. The suiting reaction mechanisms are as follows: 1) the maleic anhydride ring was completely opened by a Lewis acid catalyst (in this case, $AlCl_3$); 2) the fromation carboxyl-terminated functional groups were then covalently grafted to the

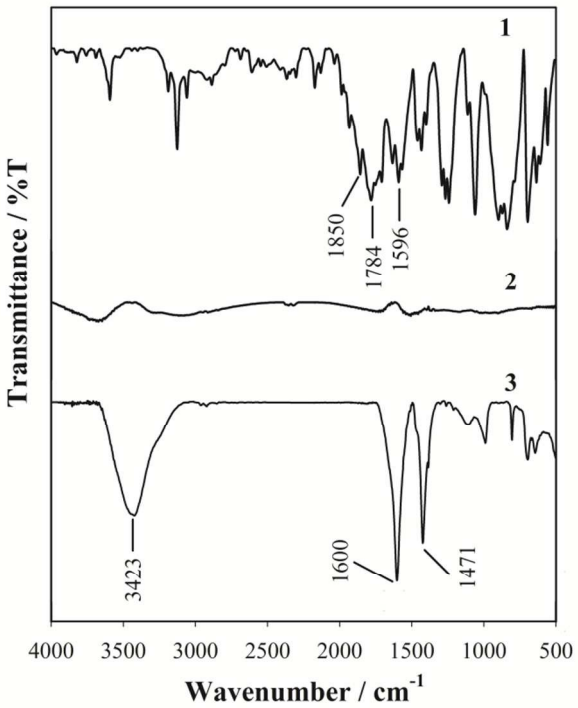

Figure 1. FTIR spectra of maleic anhydride (1), pristine CNT (2) and CNT-C (3).

sidewalls of the CNT and following reacted with the added KOH solution to form carboxylate ion. Moreover, the surface properties of PtRu/CNT-C were also characterized by FTIR spectroscopy (see the supporting information, Figures S1). It is clearly that the characteristic absorption peaks of carboxylate ion appeared in FTIR spectroscopy of PtRu/CNT-C, indicated covalently grafted functional groups still exist on CNT-C surface after depositing PtRu nanoparticles.

On the other hand, XPS was also utilized to intuitively evaluate the concentrations of the oxygenated functional groups on CNT-C. As shown in Figure 2a-b, the C1s peak (284.7 ev) and O1s peak (532.4 ev) [41] can be clearly observed, and the C/O ratio of CNT-C and AO-CNT were 31.9 and 43.1, respectively. The smaller C/O ratio of CNT-C means its higher concentrations of the oxygenated functional groups than AO-CNT. In the high-resolution C1s spectrum of the SNE-CNTs (Figure 2c-d), the peak at 284.7 eV corresponds to sp^2-hybridized graphitic carbon atoms. The small peaks at 285.9, 287.4, 289.1 and 291.3 eV obtained by peak fitting are assigned to C-O, C=O, O-C=O and π-π* bond, respectively [41]. It is interesting to note that the CNT-C have higher intensity of the O–C=O bond peak (289.1 eV) than AO-CNT, which indicated higher surface concentrations of carboxyl groups on CNT-C.

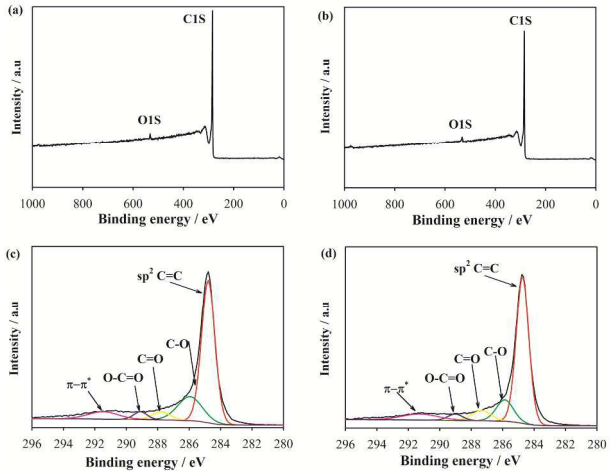

Figure 2. XPS wide scan spectra and curve fitting of the C1s peak of FTIR spectra of CNT-C (a, c) and AO-CNT (b, d).

To analyze the structure of the resultant functionalized-CNT, the CNT-C and AO-CNT were further investigated with Raman spectroscopy (Figure 3). It is noted that the peak at 1320 cm^{-1} should be assigned to the A_{1g} breathing mode of disorder graphite structure (i.e., the D band), and the peak at ~1564 cm^{-1} assigned to the E_{2g} structure mode of graphite (i.e., the G band) [32, 38]. The G band reflects the structure of the sp^2 hybridized carbon atoms. An additional side band at ~1600cm^{-1} was also observed, which is assigned as the D′ band. Both the D and the D′ bands are due to the defect sites in the hexagonal framework of graphite materials. The extent of the defects in graphite materials can be quantified by the intensity ratio of the D to G bands (i.e., I_D/I_G) [3, 12, 32, 38]. It can be obtained from Figure 2 that the values of the I_D/I_G ratio are 1.27, 1.36 and 1.65 for the pristine CNT, CNT-C and AO-CNT, respectively. The I_D/I_G value for the pristine CNT (1.27) is close to that reported in literature [3]. It is noted that the values of I_D/I_G ratio of both CNT-C and AO-CNT are higher than that of the pristine CNT because of the surface modification. However, the AO-CNT has a higher I_D/I_G ratio than the CNT-C, suggesting that the harsh chemical acid treatment causes more obvious structural damage of CNT. The results from Raman spectra revealed that the Friedel-Crafts reaction process leads to the less structural damage of CNT

than the typical acid-oxidized treatment due to its more-milder conditions. The CNT-C should save better electric conductivity than the AO-CNT, and more suitable support noble metal nanoparticles for fuel cells.

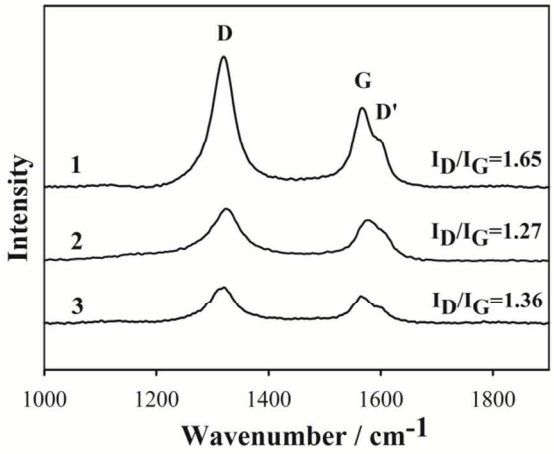

Figure 3. Raman spectrum of the AO-CNT (1), pristine CNT (2) and CNT-C (3).

As mentioned above, the excellent dispersibility of CNT in solvents for offering enough accessible specific surface areas is one of the key issues for uniform growth of metal nanoparticles. Here, a comparsion of the dispersibility of CNT-C and pristine CNT in water was carried out and the corresponding results are shown in Figure 4. Obviously, CNT-C can easily and uniformly disperse in water. In contrast, it is hard for pristine CNT to uniformly disperse in water and the aggregation and precipitation are observed. This implies the dispersibility of CNT-C in water is greatly improved in comparison with pristine CNT, which result from the hydrophilic carboxylate ions interacting with water and so preventing aggregation of CNT. The more hydrophilic materials will also lead to higher dispersion than hydrophobic ones for anchoring and growing more metal nanoparticles. It was expected that PtRu nanoparticles will be dispersed uniformly on the CNT-C with small particle size and narrow size distribution.

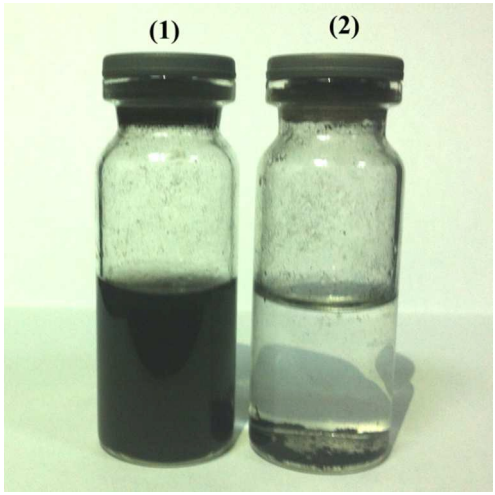

Figure 4. Digital photographs of 10 wt.% CNT-C (1) and pristine CNT (2) dispersed in water for one month.

Characterization of PtRu/CNT-C catalyst– Figure 5 shows the transmission electron microscopy (TEM) images of the PtRu/CNT-C and PtRu/AO-CNT nanohybrids. As shown in Figure 4, the CNT-C is successfully decorated with lots of well-dispersed PtRu nanoparticles. The TEM images with higher magnification of PtRu/CNT-C have also been provided (see the supporting information, Figures *S2*). Their size distribution was evaluated statistically through measuring the diameter of 200 PtRu nanoparticles in the selected TEM images and the corresponding particle size distribution were shown in Figure *S3*. It is noted the particle size of PtRu nanoparticles distributes mainly between 1.7 nm and 4.8 nm (with an average diameter of ca. 3.3 ± 0.5 nm). Noteworthy is that no nanoparticles aggregation is observed obviously on the CNT surface. However, for the AO-CNT, PtRu nanoparticles' dispersion is not satisfactory and has a broad distribution (1.5-9.5 nm) with an average diameter of ca. 5.5 ± 1.5 nm. The reasons should be as follows: for the acid-oxidized CNT, only a limited and uneven distribution of carboxyl groups generated on the defects sites of the CNT surface. When PtRu nanoparticles are deposited on the CNT surface, there are not enough and uniform carboxyl groups to anchor Pt and Ru precursors and PtRu nanoparticles, leading to poor dispersion and extensive aggregation of PtRu nanoparticles on the surface of CNT-AO. However, for the CNT-C, a large number of carboxyl groups with uniform distribution are introduced by a direct Friedel-Crafts reaction that serve as the functional groups for immobilizing Pt and Ru precursors on the CNT surface through electrostatic and coordinatic interaction. Therefore, PtRu nanoparticles on the surface of the CNT-C have a much more uniform distribution, which is more effective catalyst supports than CNT-AO.

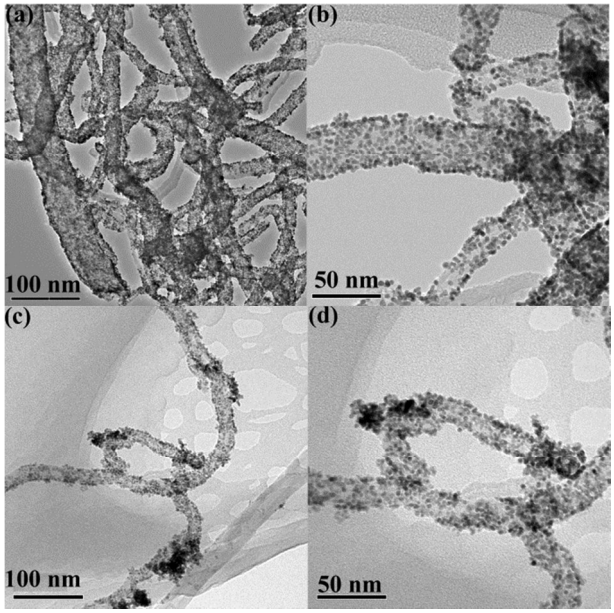

Figure 5. TEM images of PtRu/CNT-C (a, b) and PtRu/AO-CNT (c, d) nanohybrids.

Figure 6 shows the XRD patterns of PtRu nanoparticles deposited on CNT-C and AO-CNT. The diffraction peaks located at 25.0° originates from the graphitic carbon of CNTs. The presence of diffraction peaks at 39.0°, 45.3°, and 66.7°, which can be assigned to Pt(111), Pt(200), and Pt(220), consistent with the face-centered cubic (fcc) structure of platinum[38]. Moreover, there were no diffraction peaks for Ru or its oxides in the XRD patterns of samples, suggesting that PtRu alloys nanoparticles are at presence of the fcc structure of Pt. The Pt(110) bands at 39.0° are broader and weaker for PtRu/CNT-C than that for PtRu/AO-CNT, indicating the smaller size of PtRu nanoparticles on CNT-C. On the basis of Sherrer's equation[32, 38] through line broadening

of the Pt(220) peak, the average size of PtRu nanoparticles for PtRu/CNT-C and PtRu/AO-CNT was calculated as 3.5 and 5.2 nm, respectively. These values agree with the TEM results.

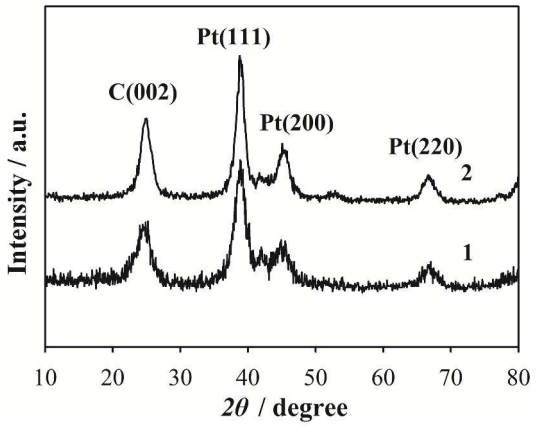

Figure 6. XRD pattern of PtRu/CNT-C (1) and PtRu/AO-CNT (2) nanohybrids.

The electrochemical surface area (ESA) provides important information regarding the number of available electrochemical active sites on the catalysts surface and at the same time accounts for the access of a conductive path available to transfer electrons to and from the electrode surface. Figure 7 shows the cyclic voltammograms (CVs) of PtRu/CNT-C and PtRu/AO-CNT nanohybrids measured in nitrogen-saturated 0.5 M H_2SO_4 solutions. Well-defined CVs are obtained in all PtRu catalyst samples. The cathodic and anodic peaks appearing between -0.25 and 0.10 V originate from the adsorption and desorption of atomic hydrogen in acidic media. Figure 7 clearly shows that PtRu/CNT-C have higher integrated peak area than PtRu/AO-CNT, which is commonly used to give the mount of adsorption-desorption charges. Based on the hydrogen adsorption-desorption charges, the values of the ESA of PtRu nanoparticles supported on the CNT-C and AO-CNT could be calculated: [42]

$ESA=Q_H/(0.21\times[Pt])$

where Q_H ($mC.cm^{-2}$) represents the mean value between the amounts of charge exchanged during the electro-adsorption and desorption of H_2 on Pt sites, [Pt] is the Pt loading ($mg.cm^{-2}$) on the electrode and 0.21 ($mC.cm^{-2}$) represents the charge required to oxidize a monolayer of H_2 on bright Pt. Results show that the ESA value of

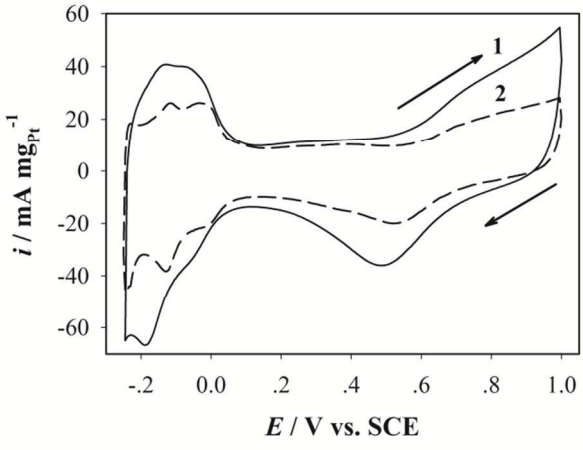

Figure 7. Cyclic voltammograms of PtRu/CNT-C (1) and PtRu/AO-CNT (2) nanohybrids in nitrogen-saturated 0.5 M H_2SO_4 aqueous solution at a scan rate of 50 mVs^{-1}.

the PtRu/CNT-C catalyst (66.2 $m^2.g^{-1}$ Pt) is larger than that of PtRu/AO-CNT catalyst (48.4 $m^2.g^{-1}$ Pt) and PtRu/C catalyst (16.5 $m^2.g^{-1}$ Pt) reported previously [38], which is attributed to the smaller particle size and much better dispersion of PtRu nanoparticles on the CNT-C, and the higher electron conductivity of CNT-C because of the much lower defect. This also demonstrates that the PtRu nanoparticles deposited on the CNT-C are electrochemically more accessible, which is very important for electrochemical oxidation of methanol.

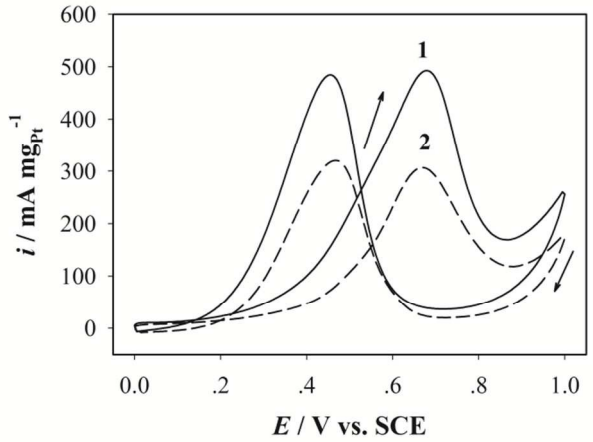

Figure 8. Cyclic voltammograms of PtRu/CNT-C (1) and PtRu/AO-CNT (2) nanohybrids in nitrogen-saturated 0.5 M H_2SO_4 + 1.0 M CH_3OH aqueous solution at a scan rate of 50 mVs^{-1}.

The electrochemical performance of the PtRu/CNT-C and PtRu/AO-CNT catalysts towards methanol electrooxidation was examined by cyclic voltammetry in nitrogen-saturated 0.5 M H_2SO_4 + 1.0 M CH_3OH aqueous solution and the corresponding results are shown in Figure 8. Comparing PtRu/AO-CNT catalyst, the significant enhancement of the peak current of methanol oxidation can be observed on the PtRu/AO-CNT catalyst. It is noted that the onset potential of methanol oxidation shifts more than 100 mV in negative direction when the catalyst support is changed from the AO-CNT to the CNT-C. On the other hand, the mass activity of methanol oxidation on PtRu/CNT-C catalyst is 496.3 $mA{\cdot}mg^{-1}$, being 1.6 and 5.0 times higher than that on PtRu/AO-CNT catalyst (304.1 $mA{\cdot}mg^{-1}$) and PtRu/C catalyst (98.3 $mA{\cdot}mg^{-1}$) reported previously [38]. Also, the mass activity for methanol oxidation of PtRu/CNT-C nanohybrids is higher than those of recent state-of-art Pt-based nanomaterials, such as PtRu/CNTs-PTCA [12], Pt-PVP-MWCNTarc [32], PtRu/1-AP-MWCNTs [38], PtRu/CNTs-PIL [2]. The specific activity, defined by current normalizing to the ESA value of catalysts, was also employed to further investigate the nature catalytic activity of the obtained nanohybrids (Figure *S4*). It was found that PtRu/CNT-C catalyst also have a higher specific activity (7.4 A m^{-2}) than that of PtRu/AO-CNT catalyst (6.3 $A{\cdot}m^{-2}$). In addition, as indicated by the dotted lines in Figure *S4*, the corresponding potential of PtRu/CNT-C is much lower than that of PtRu/AO-CNT, further demonstrating that PtRu/CNT-C at a given oxidation current density, have a significantly enhanced electrocatalytic activity.

In practical application, the long-term cycle stability of the catalysts is of great importance [43]. In this work, the long-term cycle stabilities of PtRu/CNT-C and PtRu/AO-CNT catalysts have been

investigated in 0.5M H_2SO_4 + 1.0M CH_3OH aqueous solution by cyclic voltammetry and the corresponding results are shown in Figure 9. From Figure 9, it can be observed that the value of $i_{pI}/i_{pI(1)}$ decreases gradually with the successive scan. In the case of PtRu/CNT-C nanohybrids, the peak current at 600th cycle is about 89% of that measured at the first cycle. The decrease of $i_{pI}/i_{pI(1)}$ on PtRu/CNT-C is only 11% for 600 cycles. However, for the PtRu/AO-CNT catalyst, a large decrease (27%) is found. To further eliminate the effects of the decrease of methanol concentration on the decay of the peak current, we replaced methanol solution with fresh solution after 600 cycles and the recovery peak current was recorded (Figure *S5*). It is noted that for the PtRu/CNT-C electrocatalyst, the oxidation peak current can recover within 600 cycles and about 6 % loss occurs after 600 cycles; however, for the PtRu/AO-CNT electrocatalyst, the recovery of the peak current can be observed 18 % loss occurs after 600 cycles. The improved durability of the PtRu/CNT-C catalyst was attributed to the high density of functional groups, the integrity structural and the high corrosion resistance of CNT-C, which helps to inhibit PtRu nanoparticles dissolution, ripening and aggregation.

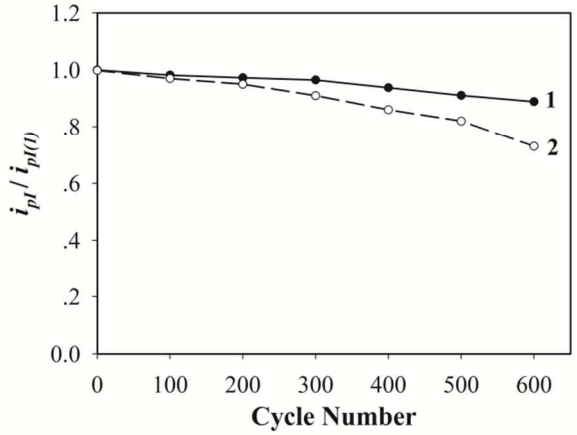

Figure 9. Long-term cycle stabilities of PtRu/CNT-C (1) and PtRu/AO-CNT (2) nanohybrids in nitrogen-saturated 0.5 M H_2SO_4+ 1.0 M CH_3OH. i_{pI}, the forward peak current; $i_{pI(1)}$, the forward peak current at the first cycle.

Conclusions

In summary, we have successfully developed a simple synthetic strategy for the nobel metal nanoparticles/CNT nanohybrids with high electrocatalytic activity based on the carboxylated-carbon nanotubes. Due to enough carboxylate ion groups are introduced on the CNT surface with high density and uniform distribution, the solubility of CNT in water and its available specific surface areas have been obviously improved. Comparing to PtRu/AO-CNT nanohybrids, PtRu/CNT-C nanohybrids displayed significantly enhanced electrocatalytic activity and stability toward methanol oxidation, which is because of the smaller particle size and higher dispersion of PtRu nanoparticles on CNT-C, and stronger interaction between PtRu nanoparticles and CNT-C. The CNT-C should be a promising catalyst support for noble metal nanoparticles in fuel cells.

Acknowledgements

This work was financially supported by National Natural Science Foundation of China (21303134), China Postdoctoral Science Foundation (2013M532017) and Natural Science Foundation of Shaanxi Province, China (2014JQ2046).

Notes and references

[a] Key Laboratory of Applied Surface and Colloid Chemistry, Ministry of Education and College of Chemistry and Chemical Engineering, Shaanxi Normal University, Xi'an, 710119, PR China; Tel./Fax: +86-29-85310825; E-mail address: c.wang@snnu.edu.cn.

[b] College of Chemistry and Chemical Engineering, Xi'an University of Science and Technology, Xi'an, 710054, PR China; E-mail address: wubohua2005@126.com.

[c] College of Chemistry and Chemical Engineering, Hunan Normal University, Changsha, 410081 PR China.

† Electronic Supplementary Information (ESI) available: [ICP-AES analysis of electrocatalysts (Table S1); FTIR spectra of PtRu/CNT-C (Figure S1); TEM images of PtRu/CNT-C nanohybrids (Figure S2); Size distribution of PtRu nanoparticles of PtRu/CNT-C and PtRu/AO-CNT nanohybrids (Figure S3); Cyclic voltammograms (specific activity) and Linear sweep voltammetry of PtRu/CNT-C and PtRu/AO-CNT nanohybrids in nitrogen-saturated 0.5 M H_2SO_4 + 1.0 M CH_3OH aqueous solution at a scan rate of 50 mVs^{-1} (Figure S4 and S5); Comparison of the forward peak current at the first cycle (i_0) and recovery forward peak current (i_R) in the fresh methanol solution after long-term cyclic voltammograms scanning experiments (600 cycles) on PtRu/CNT-C and PtRu/AO-CNT nanohybrids (Figure S6)]. See DOI: 10.1039/b000000x/

1. S. Iijima, Nature, 1991, **354**, 56-58.
2. H. Chu, Y. Shen, L. Lin, X. Qin, G. Feng, Z. Lin, J. Wang, H. Liu and Y. Li, *Adv. Funct. Mater.*, 2010, **20**, 3747-3752.
3. B. Wu, D. Hu, Y. Kuang, B. Liu, X. Zhang and J. Chen, *Angew. Chem. Int. Ed.*, 2009, **48**, 4751-4754.
4. L. Qu, L. Dai and E. Osawa, *J. Am. Chem. Soc.*, 2006, **128**, 5523-5532.
5. R. Chetty, S. Kundu, W. Xia, M. Bron, W. Schuhmann, V. Chirila, W. Brandl, T. Reinecke and M. Muhler, *Electrochim. Acta*, 2009, **54**, 4208-4215.
6. K. M. Samant, V. S. Joshi, G. Sharma, S. Kapoor and S. K. Haram, *Electrochim. Acta*, 2011, **56**, 2081-2086.
7. L. Yang, J. Chen, X. Wei, B. Liu and Y. Kuang, *Electrochim. Acta*, 2007, **53**, 777-784.
8. Z. He, J. Chen, D. Liu, H. Zhou and Y. Kuang, *Diamond Relat. Mater.*, 2004, **13**, 1764-1770.
9. B. Wu, C. Wang, D. Xue and J. Xiao, *Diamond Relat. Mater.*, 2014, **46**, 1-7.
10. Y. S. Chun, J. Y. Shin, C. E. Song and S.-g. Lee, *Chem. Commun.*, 2008, 942-944.
11. R. B. Rakhi, K. Sethupathi and S. Ramaprabhu, *J. Phys. Chem. B*, 2009, **113**, 3190-3194.
12. B. Wu, D. Hu, Y. Kuang, Y. Yu, X. Zhang and J. Chen, *Chem. Commun.*, 2011, **47**, 5253-5255.
13. J. Zhang, S. Guo, J. Wei, Q. Xu, W. Yan, J. Fu, S. Wang, M. Cao and Z. Chen, *Chem. Eur. J.*, 2013, **19**, 16087-16092.
14. L. Y. Zhang, C. X. Guo, Z. Cui, J. Guo, Z. Dong and C. M. Li, *Chem. Eur. J.*, 2012, **18**, 15693-15698.
15. S. P. Somani, P. R. Somani, A. Sato and M. Umeno, *Diamond Relat. Mater.*, 2009, **18**, 497-500.
16. J. M. Sieben and M. M. E. Duarte, *Int. J. Hydrogen Energy*, 2012, **37**, 9941-9947.

17. S. Zhang, Y. Shao, G. Yin and Y. Lin, *J. Mater. Chem.*, 2010, **20**, 2826-2830.
18. C.-T. Hsieh, W.-Y. Chen, I. L. Chen and A. K. Roy, *J. Power Sources*, 2012, **199**, 94-102.
19. S. Jiang, L. Zhu, Y. Ma, X. Wang, J. Liu, J. Zhu, Y. Fan, Z. Zou and Z. Hu, *J. Power Sources*, 2010, **195**, 7578-7582.
20. D. Morales-Acosta, M. D. Morales-Acosta, L. A. Godinez, L. Álvarez-Contreras, S. M. Duron-Torres, J. Ledesma-García and L. G. Arriaga, *J. Power Sources*, 2011, **196**, 9270-9275.
21. M. Sakthivel, A. Schlange, U. Kunz and T. Turek, *J. Power Sources*, 2010, **195**, 7083-7089.
22. Y. Shao, G. Yin, J. Wang, Y. Gao and P. Shi, *J. Power Sources*, 2006, **161**, 47-53.
23. J. M. Sieben, A. Ansón-Casaos, M. T. Martínez and E. Morallón, *J. Power Sources*, 2013, **242**, 7-14.
24. V. Baglio, C. D'Urso, D. Sebastián, A. Stassi and A. S. Aricò, *Int. J. Hydrogen Energy*, 2014, **39**, 5399-5405.
25. A. O. Neto, R. R. Dias, M. M. Tusi, M. Linardi and E. V. Spinacé, *J. Power Sources*, 2007, **166**, 87-91.
26. Y.-X. Wang, H.-J. Zhou, P.-C. Sun and T.-H. Chen, *J. Power Sources*, 2014, **245**, 663-670.
27. H. Huang, Q. Chen, M. He, X. Sun and X. Wang, *J. Power Sources*, 2013, **239**, 189-195.
28. X. Peng, J. Chen, J. A. Misewich and S. S. Wong, *Chem. Soc. Rev.*, 2009, **38**, 1076-1098.
29. D. Eder, *Chem. Rev.*, 2010, **110**, 1348-1385.
30. B. Wu, Y. Kuang, X. Zhang and J. Chen, *Nano Today*, 2011, **6**, 75-90.
31. M. Rahsepar, M. Pakshir, Y. Piao and H. Kim, *Electrochim. Acta*, 2012, **71**, 246-251.
32. Y. L. Hsin, K. C. Hwang and C.-T. Yeh, *J. Am. Chem. Soc.*, 2007, **129**, 9999-10010.
33. H. S. Park, B. G. Choi, S. H. Yang, W. H. Shin, J. K. Kang, D. Jung and W. H. Hong, *Small*, 2009, **5**, 1754-1760.
34. G. G. Wildgoose, C. E. Banks and R. G. Compton, *Small*, 2006, **2**, 182-193.
35. N. Mackiewicz, G. Surendran, H. Remita, B. Keita, G. Zhang, L. Nadjo, A. s. Hagège, E. Doris and C. Mioskowski, *J. Am. Chem. Soc.*, 2008, **130**, 8110-8111.
36. M. Okamoto, T. Fujigaya and N. Nakashima, *Small*, 2009, **5**, 735-740.
37. Y. Cheng and S. P. Jiang, *Electrochim. Acta*, 2013, **99**, 124-132.
38. S. Wang, X. Wang and S. P. Jiang, *Langmuir*, 2008, **24**, 10505-10512.
39. S. Chen, Z. Wei, L. Guo, W. Ding, L. Dong, P. Shen, X. Qi and L. Li, *Chem. Commun.*, 2011, **47**, 10984-10986.
40. Z. Wang, Q. Zhang, D. Kuehner, X. Xu, A. Ivaska and L. Niu, *Carbon*, 2008, **46**, 1687-1692.
41. Y.-L. Huang, S.-M. Yuen, C.-C. M. Ma, C.-Y. Chuang, K.-C. Yu, C.-C. Teng, H.-W. Tien, Y.-C. Chiu, S.-Y. Wu, S.-H. Liao and F.-B. Weng, *Compos. Sci. Technol.*, 2009, **69**, 1991-1996.
42. A. Pozio, M. De Francesco, A. Cemmi, F. Cardellini and L. Giorgi, *J. Power Sources*, 2002, **105**, 13-19.
43. B. Wu, D. Hu, Y. Yu, Y. Kuang, X. Zhang and J. Chen, *Chem. Commun.*, 2010, **46**, 7954-7956.